J Polym Res (2013) 20:194
DOI 10.1007/s10965-013-0194-5

ORIGINAL PAPER

Effects of various polyolefin copolymers on the interfacial interaction, microstructure and physical properties of cyclic olefin copolymer(COC)/graphite composites

Alper Kaşgöz · Dinçer Akın · Ali Durmus · Nevra Ercan · Faruk Öksüzömer · Ahmet Kaşgöz

Received: 6 February 2013 / Accepted: 9 June 2013 / Published online: 20 June 2013

Abstract In this study, effects of various types of functional polyolefin copolymers (FPOCs), poly(isobutylene-*alt*-maleic anhydride), poly(maleic anhydride-*alt*-1-octadecene) and poly(ethylene-*graft*-maleic anhydride), on the microstructure formation, interfacial interaction and physical properties of cyclic olefin copolymer (COC)/graphite composites were investigated. The COC/graphite composites were prepared in a lab. scale twin screw extruder. Microstructural features of samples were studied in a field emission scanning electron microscopy (FESEM). Viscoelastic properties of samples, obtained from the rheology tests in melt state and the dynamic mechanical analysis in solid state were used to quantify interfacial interactions between the COC and graphite depending on the types of FPOC. The average aspect ratio (A_f) values of graphite flakes in the COC phase were determined about 40–65 by SEM observation and image analysis study on the samples prepared with different types of FPOC. Based on the gas permeability measurements, tortuous diffusion model suggested that the A_f values of graphite flakes varied between 40 and 80 depending on the amount of graphite. It was shown that the poly(isobutylene-*alt*-maleic anhydride) copolymer provided relatively higher interfacial interaction between the COC and graphite flakes than the other FPOCs.

Keywords Cyclic olefin copolymer · Polyolefin copolymer · Graphite · Composite · Interface

A. Kaşgöz · D. Akın · A. Durmus (✉) · N. Ercan · F. Öksüzömer · A. Kaşgöz
Department of Chemical Engineering, Istanbul University, Faculty of Engineering, 34320 Avcılar, Istanbul, Turkey
e-mail: durmus@istanbul.edu.tr

Introduction

Polymer composites reinforced with various types of carbon fillers have gained a considerable interest due to their superior physical properties such as high electrical and thermal conductivity, improvement in mechanical performance, low weight and excellent resistance to corrosive environments and chemicals. Most of the relevant studies have focused on the preparation of electrically conductive composites. Some possible applications of such composites include electromagnetic (EMI) and radio frequency interference (RFI) materials, parts of electronic devices and batteries, sensors, actuators and corrosion-resistant coatings etc.

Various forms of carbon such as carbon black (CB), single or multi-walled carbon nanotubes (SWCNT, MWCNT), carbon fibers (CF), fullerenes (FL) and graphite (G) have been used in polymer/carbon composites. Especially carbon nanotubes have generated great scientific attention since they promise excellent physical performance with very low loading amounts compared to other carbon types. But, structural uniformity, difficulties in mass production and cost of carbon nanotubes have been considered as serious drawbacks for their industrial usage in low-cost composites.

On the other hand, graphite, cheap and available in large quantity, is the practical, cost-conscious material alternative for the mass production of high performance or conductive composites [1]. Graphite is a two-dimensional (2D) carbon filler formed by the stacks of one-atom-thick planar graphene sheets of densely packed carbon atoms in a honeycomb crystal lattice [2]. As a 2D filler, it can be used in composite formulations as pristine or modified form. Surface modification of layered graphite can be performed by several techniques such

as chemical oxidation, thermal expansion and reduction, covalently grafting of different functional groups and electrochemical modifications etc. The chemical oxidation followed by the thermal expansion/reduction is the most attractive surface modification method to prepare graphene nano-sheets [3]. This modification allows expansion of interlayer distance between the graphene nano-sheets, increasing the surface area and facilitates the dispersion of graphene sheets in a polymer matrix. For completely exfoliated graphene sheets, theoretical surface area is predicted about 2,630 m^2/g [4]. But, the conventional expansion routes (chemical or thermal) yield quite lower surface area than the theoretical value (<100 m^2/g). This implies physical difficulty for the dispersion and one-sheet-thick exfoliation of a graphite stack.

Physical properties of graphite or expanded graphite (EG) filled polymer composites have been extensively studied for many resin based thermoset [5–7] and thermoplastic polymers [8–15]. Particularly, graphite filled engineering thermoplastics or high performance polymers such as polycarbonate (PC) [16, 17], polyamides (PA) [18–20], polyphenylene sulfide (PPS) [21] and thermoplastic polyesters like poly(ethylene terephthalate) (PET) [22–24], poly(ethylene-2,6-naphthalate) (PEN) [25] and polyethersulfone (PES) [26] have offered innovative applications because such composites can provide the sufficient electrical conductivity and excellent mechanical performance. But, dispersion of graphite flakes into a thermoplastic matrix by melt processing methods is an important challenge similarly another layered materials, clays and layered double hydroxides (LDHs). Modification of graphite surfaces normally revealed some extra processing steps, difficulties and costs. Hence, using of natural or unmodified graphite flakes and conventional melt processing methods can be considered the simplest route to prepare composite structures with enhanced physical properties. On the other hand, natural or unmodified graphite could lead to formation of some structural and physical defects in a polymer based composite, for example, poor dispersion and interfacial adhesion and resulted deterioration in some physical performances. Therefore, quantifying of interfacial interaction between natural graphite flakes and polymer phase is an important research area to prepare high performance composites with enhanced physical properties, especially for highly hydrophobic and non-polar polymers like polyolefins.

Many studies have been published on the enhancement of interfacial interaction between the polymer phase and graphite/graphene flakes [14, 27–30]. Many of these studies have focused on the effects of surface modification of graphite flakes on the graphite dispersion and resulted physical properties of composites. Recently, Wu et al. studied on a route to improve interfacial interactions in graphite filled poly(methylmethacrylate) (PMMA) composites by grafting of 3-aminopropyltriethoxsilane (APTS) on the expandable graphite surfaces [28]. Kim and Park prepared aminized graphite nanosheets to increase interfacial interactions in PMMA/graphite composites [29]. Cai and Song suggested a simple and effective route, creating a crystalline polymer layer on the surface of graphite oxide nanoplatelets by thermal treatment, to enhance the interface between graphite oxide nanoplatelets and a semi-crystalline polymer [30].

Only a few studies have been published on the improvement of interfacial interactions in the graphite filled thermoplastic based composites by using functional polymeric additives. Cerezo et al. investigated morphology, thermal stability and mechanical behavior of poly(propylene)-*grafted*-maleic anhydride (PP-*g*-MA)/layered expanded graphite oxide (EGO) composites prepared by solution blending [31]. They suggested that hydrogen bonding of polar groups between PP-*g*-MA and EGO increased the mechanical properties of samples. Mirzazadeh et al. studied the effect of interface and degree of interfacial interaction upon electrical conductivity and dispersion state of graphite nanosheets in polypropylene (PP)/(EG) composites prepared with melt processing method and including maleic anhydride grafted polypropylene (PP-*g*-MA) and maleic anhydride grafted ethylene-propylene-diene monomer (EPDM-*g*-MA) as compatibilizers [32]. They reported that the conductivity threshold was controlled by the extent of interfacial interaction between PP and EG and higher level of interaction between PP and EG which refer to better dispersion of the EG nanolayers in the polymer matrix and therefore better conductivity was obtained by using the PP-*g*-MA as compatibilizer. On the other hand, they also reported that high level of compatibilizer could reduce the electrical conductivity by forming the separated aggregates of EG covered well with the compatibilizer.

Cyclic olefin copolymers (COCs) are new types of amorphous engineering thermoplastics obtained from the copolymerization of ethylene and cyclic olefins [33]. The chemical structure of a COC consisting of ethylene and norbornene units can be seen in Table 1. The COCs are generally characterized by excellent transparency, superior mechanical properties and solvent resistance. Depending on the mole or weight ratio of the ethylene units in the structure, they also exhibit relatively high glass transition temperatures, ranged between 80 and 180 °C, compared to other polyolefins and thus long service life without a loss in physical properties. Beside the excellent physical properties of COCs, one of the important advantages of such polymers is their melt processability. There are many actual and promising applications for the COCs in the medical, optical, film and packaging areas.

Although preparation and physical properties of COC composites including various types of nano-size inorganic fillers such as silica [34, 35], titania (TiO_2) [36] and polyhedral oligomeric silsesquioxanes (POSS) [37] have been studied, only few works have been reported on the preparation and characterization of COC composites filled with carbon based fillers. Motlagh et al. prepared a series of composites

Table 1 Chemical structures, commercial names and some physical properties of the materials used in the study

	Polymer	Functional polyolefin copolymers			Filler
	Cyclicolefin copolymer COC	Poly(isobutylene-*alt*-maleic anhydride) C1	Poly(maleic anhydride-*alt*-1-octadecene) C2	Polyethylene-*graft*-maleic anhydride C3	Graphite G
Commercial name	TOPAS® 8007	Aldrich 531278	Aldrich 419117	Aldrich 456632	TIMREX® KS75
Chemical structure	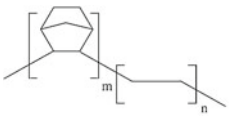	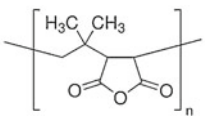	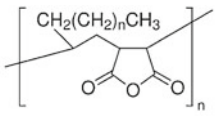	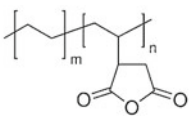	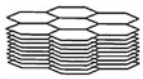
Density (g/cm^3)	1.02	1.30	0.97		2.24
T_g[a] (^{o}C)	78	141	120-130[d]	105[f]	
MVR[b] (ml/10min.)	32	M_w: ~ 6000	M_n: 30000-50000	MAh[g]: 3.0	
Surface Area (m^2/g)					6.5
Particle size (d_{90})					55.8μm
OAN[c] (ml/100mg)			AN[e]: 310-315	AN: 32-36	84

[a] Glass transition temperature measured with DSC method

[b] Melt volume flow index under the test conditions of 260 °C and 2.16 kg (ISO 1133)

[c] Oil adsorption number (ASTM)

[d] Softening point

[e] Acid number (mg KOH/g)

[f] Melting temperature measured with DSC method

[g] Maleic anhydride graft ratio (%)

containing CF and CB by melt compounding and investigated the electrical and rheological properties of the COC/carbon composites [38]. In our previous paper, microstructure and rheological properties of COC/G and EG composites were reported, in detail [39].

To the best of our knowledge, no paper has yet been published about the effects of functional copolymers on the physical properties of graphite filled COC composites. In this study, microstructural, rheological and physical properties of series of COC/graphite composites including different types and amount of functional polyolefin copolymers (FPOCs) were investigated, in detail. Effects of chemical and physical features of polyolefin copolymers on the interfacial interactions between COC phase and graphite surfaces were quantified.

Experimental

Materials

The COC used in this study was a commercial grade copolymer, Topas® 8007, kindly donated by Ticona. The FPOCs used in the study were poly(isobutylene-*alt*-maleic anhydride), poly(maleic anhydride-*alt*-1-octadecene) and poly(ethylene-*graft*-maleic anhydride). Commercially available graphite, TIMREX® KS75, was kindly provided by TIMCAL (Bodio, Switzerland). Some physical properties of the copolymers and graphite employed in the study are listed in Table 1.

Sample preparation

Composite samples were prepared by the melt processing method in a lab-scale, co-rotating twin screw extruder (Rondol Micro Lab., UK, *D*:10 mm, *L*/*D*: 20) with a screw speed of 50 rpm. Intermeshing screws of the extruder were configured as including 3D of 4×60° followed by 2D of 4×90° kneading segments. A temperature profile of 185-200-220-220 °C was applied throughout the barrel from the feeding zone to die. A rod die with the diameter of 2 mm, was used. Extrudates were granulated and used in the melt rheology tests. Before the melt processing, graphite was dried in a vacuum oven overnight at 70 °C. The COC, Topas® 8007, was also processed at the same conditions. Sample compositions are listed in Table 2. The sample abbreviations directly refers to composition, e.g. the C2-G15 corresponds to the sample prepared with the poly(maleic anhydride-*alt*-1-octadecene) as compatibilizer which is defined as C2 in Table 1, including of 15 phr (part per hundred of polymer) of graphite. The amount of FPOC was also increased with the increasing amount of graphite in the samples to keep the FPOC/graphite ratio, (1:1 in w/w), constant.

Structural and physical characterization of samples

Microstructural features of the graphite and composite samples were characterized by a field emission scanning electron microscope (FESEM, FEI Quanta FEG 450). Cryo-fractured surfaces of the samples were directly imaged in the electron microscope after a proper sample preparation of sputter-coated with gold.

Table 2 Sample compositions

Series	Samples	COC	C1	C2	C3	Graphite (phr*)
G-x	G0	100				
	G5	100				5
	G10	100				10
	G15	100				15
C1-x	C1-G5	95	5			5
	C1-G10	90	10			10
	C1-G15	85	15			15
C2-x	C2-G5	95		5		5
	C2-G10	90		10		10
	C2-G15	85		15		15
C3-x	C3-G5	95			5	5
	C3-G10	90			10	10
	C3-G15	85			15	15

* part per hundred of polymer

Viscoelastic behavior of the samples was analyzed by a dynamic oscillatory rheometer in the melt state. A controlled strain rheometer (AR-G2, TA Instruments) equipped with 25 mm diameter parallel plate geometry was employed for the rheology tests. Samples were directly loaded and molded between the plates and rheological tests were carried out at 200 °C with a gap distance of 1 mm under nitrogen atmosphere. First, strain sweep test was performed from the initial strain value of 0.01 % to the final strain value of 10 % with the angular frequency of 1 rad/s to determine the linear viscolelastic (LVE) region of the samples. Shear strain was applied in the range of 0.1–100 % for the COC. Storage (G') and loss (G'') modulus of the samples were recorded as a function of shear strain (γ %). In the frequency sweep tests, a small amplitude oscillatory shear was applied to the samples. The G', G'' and dynamic viscosity (η^*) were measured as a function of angular frequency (ω) in the range of 0.1–100 rad/s at a strain value in the LVE region (strain magnitude of 10 % for the COC and 0.5 % for the composites).

Thermal properties of the samples were analyzed in a heat-flux type differential scanning calorimeter (DSC), SII Nanotechnology ExStar 6200. Temperature and heat flow calibration of the instrument were achieved with high purity indium (In), tin (Sn) and zinc (Zn) metals. Samples weighing about 7–8 mg in an aluminum crucible were heated from 0 °C to 200 °C with the heating rate of 10 °C min^{-1} under nitrogen (N_2) atmosphere at a flow rate of 50 ml min^{-1} to prevent thermal degradation of the samples.

Dynamic mechanical analysis (DMA) of the film samples prepared in a hot press was performed with a DMA (ExStar 6100, SII Nanotechnology). The height and width of the test specimens were 20 and 10 mm, respectively. The DMA test was performed in tension mode at a frequency of 1.0 Hz and the temperature range of 20–300 °C with the heating rate of 2 °C/min.

Gas permeability tests were performed with a permeability testing apparatus, GDP C-2000 (Brugger Feinmechanik GmBH) working according to manometric method, (ASTM 1434) at 25ºC and %50 relative humidity. Thicknesses of the test specimens, varied in the range of 120–150 μm, which were measured with a micrometer at 10 points at least, were within the ±5 %. Samples were masked by an aluminum foil for exposing the permeation area of 22.9 cm^2. Gas permeability tests were performed with an inert gas, nitrogen instead of oxygen in order to avoid possible effects of oxygen adsorption into graphite micropores and surfaces on the permeability results. Test gas (purity of 99.9 %) used in the permeation measurements was obtained from a commercial supplier. For each sample, three different films were tested and the average permeability (P) values are reported, as normalized for the film thickness of 100 μm.

Results and discussion

Microstructure of samples

SEM images of graphite particles and flakes are given in Fig. 1. In Fig. 1(b), layered and 2D structure of the graphite is clearly seen. The lateral size and thickness of the flake, marked with red lines on the images, were found to be about 14 μm and 3.5 μm, respectively. By using these values, the average aspect ratio (A_f) of the graphite flake can be calculated. The A_f is defined as the ratio of width to thickness of the filler (l/d) which is an indicative parameter for filler dispersion in composite systems. The value of A_f is equal to 1 for spherical fillers. It was found that the A_f of the pristine graphite flake was about 3–5.

SEM images of the COC/graphite and COC/FPOC/graphite samples including 5 phr of graphite are given in Fig. 2. Fig. 2(a) and (b) shows the SEM images of G5 samples at different magnifications. As seen in Fig. 2(a), graphite flakes were successfully dispersed in the COC phase. By comparing the SEM image of the G5 sample given in Fig. 2(b) to that of the pristine graphite flake given in Fig. 1, it is obviously seen that the graphite flakes in the composite sample are much thinner than that of the raw-flakes although the G5 sample does not contain a FPOC.

In this image, lateral size and thickness of the flake were determined to be 15–20 μm and 0.3 μm which correspond to the average A_f value of 50–65 for the G5 sample. This result shows that the dispersion of graphite flakes in the COC matrix is more related to the processing method and equipments rather than the compositional parameters. It can be concluded that melt blending of the COC and graphite in a co-rotating twin screw extruder with intermeshing screws

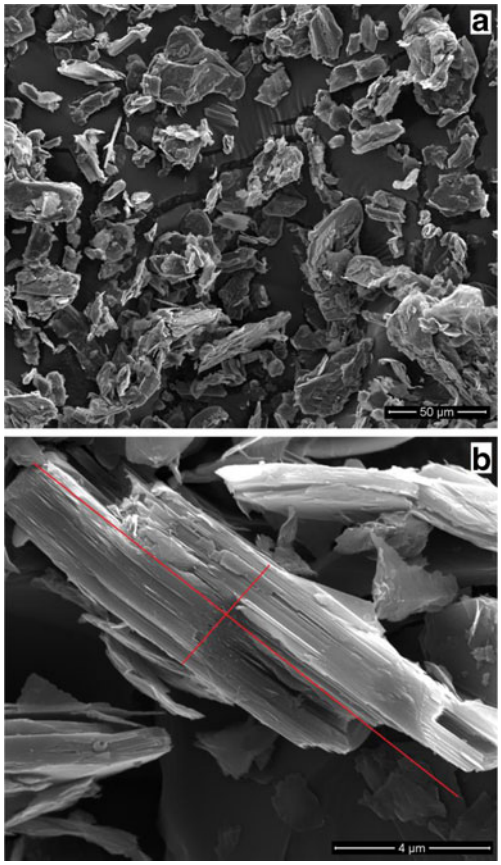

Fig. 1 SEM images of graphite particles and flakes at different magnifications

and five parts of kneading segments was sufficient tool to disperse the graphite flakes homogenously and increase the aspect ratio.

SEM images of the cross-section of C1-5 sample prepared with the poly(isobutylene-*alt*-maleic anhydride) as functional interfacial additive are seen in Fig. 2(c) and (d). One can notice that the SEM images of the C1-5 sample are quite different from those of other samples. As seen in these figures, surface of the graphite flakes which are embedded in the fractured cross-section of the sample are not smooth and covered well by the polymer matrix which suggests a strong interfacial interaction and adhesion between the graphite flakes and COC phase. Estimated average A_f value for this sample series is approximately 40, based on the SEM image analysis. The SEM images of the C1-5 sample suggest that the poly(isobutylene-*alt*-maleic anhydride) is an effective additive to increase the interfacial interaction between the natural graphite flakes and the highly hydrophobic polymer matrix, COC. Despite the slightly lower average A_f value of the C1-5 sample than the G5, it can be expected that the physical properties of the C1-x series of samples could be significantly improved compared to those of G-x and other series of samples.

Figure 2(e) and (f) show the SEM images of the C2-5 sample prepared by using of 5 wt% of poly(maleic anhydride-*alt*-1-octadecene) into the composition. It is seen in these images that the graphite flakes are dispersed well as thinner sheets than the pristine form of graphite. The A_f values of the graphite flakes seen in Fig. 2(f) was determined to be about 60 (*l*:25 µm/*d*:400–420 nm) by the SEM image analysis. But, big voids are present around the graphite flakes which points out that no interaction between the COC and graphite surfaces are gained by using of poly(maleic anhydride-*alt*-1-octadecene). Furthermore, white droplets and spherulitic holes with the average size of 1–2 µm appear in the SEM images which refer to the poly(maleic anhydride-*alt*-1-octadecene) phase. This morphology signifies that the COC and poly(maleic anhydride-*alt*-1-octadecene) is highly immiscible.

SEM images of the C3-5 sample prepared with the poly (ethylene-*graft*-maleic anhydride) copolymer are demonstrated in Fig. 2(g) and (h). Morphology of the sample is similar to that of the C2-5. The A_f values of the graphite flakes seen in Fig. 2(h) was determined to be about 50 (*l*:3-µm/*d*:60 nm) by the SEM image analysis.

Viscoelastic properties of samples

Viscoelastic properties of polymer composites can provide precise and useful information about microstructural features such as level of filler dispersion, interfacial interaction between filler and polymer phases, filler-filler interaction and/or physical percolation and processability of these materials. Viscoelastic properties of polymer composites depend on the many parameters such as type, size, geometry, amount, surface area and surface characteristics of filler, other compositional parameters like using of compatibilizer or interfacial agents and additives, processing route, thermo-mechanical history of materials and environmental effects. It is also well known that the viscoelastic properties of polymer composites are also time and temperature dependent. Therefore, quantifying the viscoelastic properties of polymer composites is quite important to understand effect of compositional parameters on the microstructure formation and related physical properties of these materials. In this study, viscoelastic properties of COC/graphite composites were studied with the rheological measurements in the melt state and DMA tests in the solid-state.

Before the rheological measurements, a time sweep test was performed with the strain amplitude of 0.05 and frequency of 1 rad/s at 200 °C for 30 min to determine the thermal stability of COC. The shear modulus values of COC (G' and G'') were recorded during the test. In time sweep test, no change was observed in the G' and G'' curves (not given here) during 30 min. which implied that the polymer matrix provided the melt stability for, at least, 30 min. Thus, it was supposed that the further rheological tests can be safely run

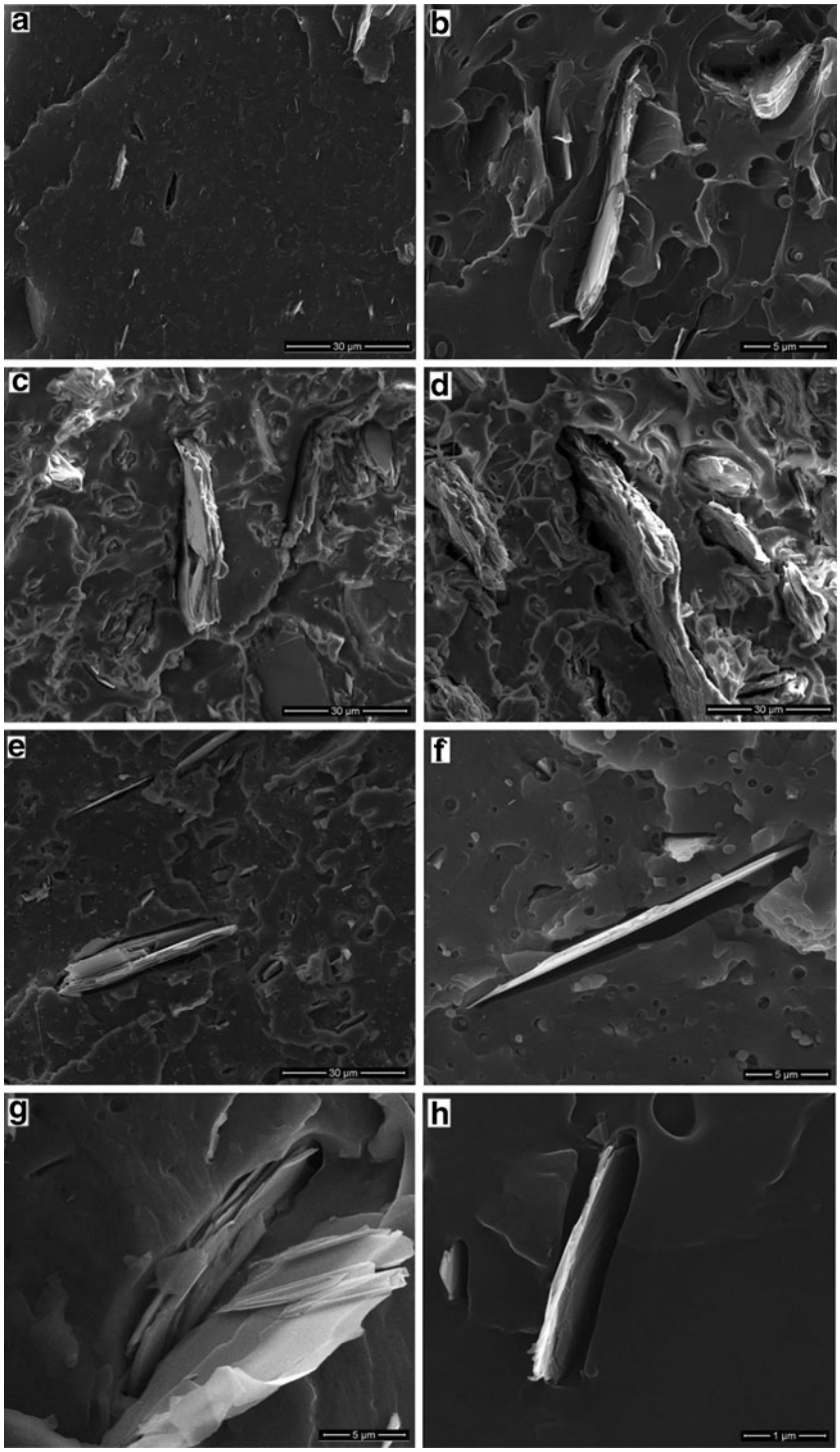

Fig. 2 SEM images of the COC/graphite composites of G5 (**a** and **b**), C1-G5 (**c** and **d**), C2-G5 (**e** and **f**) and C3-G5 (**g** and **h**) at different magnifications

by neglecting the possible degradation effects of polymer matrix on the rheological properties of samples.

Then the dynamic strain sweep test was applied to the samples to characterize strain dependence of the viscoelastic properties of the samples and determine LVE region. Since the storage modulus is more sensitive rheological function than the loss modulus to the structural and mesoscopic changes of the polymer based composite and hybrid materials, only the storage modulus curves are presented here. As an example, dependence of storage modulus (G') on the shear strain ($\gamma\%$) are given in Fig. 3 for the some samples.

Figure 3(a) illustrates the G'-$\gamma\%$ curves of the COC and COC/graphite composites prepared with the poly(isobutylene-*alt*-maleic anhydride). Storage modulus of the composite samples exhibits a linear region (Newtonian plateau or plateau modulus) at low strains and non-linear region at high strain

amplitudes. As expected, it is clearly appeared that the plateau modulus (G'_p) of the samples increases with the increasing amount of graphite. A similar trend was obtained for the sample series prepared with and without the other FPOCs, but not given here. This result typically indicates the reinforcement effect of graphite flakes on the shear modulus of COC. Figure 3(b) compares the G'-γ% curves of composites prepared with different types of FPOCs, including a constant amount of graphite (15 phr) and FPOCs (15 wt%). As seen in this figure, the highest modulus was obtained with the poly(isobutylene-*alt*-maleic anhydride). The C2-G15 sample prepared with the poly(maleic anhydride-*alt*-1-octadecene) was yielded slightly higher storage modulus than the sample of G15, prepared with the pristine graphite and included no FPOCs, but lower than the C1-G15. Interestingly, the C3-G15 sample, prepared with the poly(ethylene-*graft*-maleic anhydride) showed the lowest storage modulus among the composites including the same amount of graphite. It is well known that the poly(ethylene-*graft*-maleic anhydride) copolymers are the most effective and widely used compatibilizer or interfacial agent in the polymer composites and blends. But in the COC/graphite systems, it acts quite different from the other composite systems with various types of fillers such as, clay/organoclay, natural fibers, glass fibers, surface modified carbon based materials, natural or synthetic inorganic materials etc.

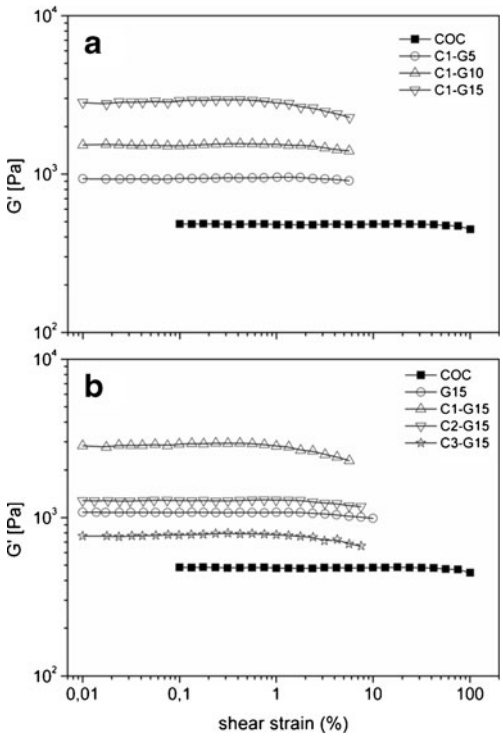

Fig. 3 Storage modulus (G') of the some samples as a function of shear strain (γ%), depending on the (**a**) graphite amount for the sample series prepared with PiB-*alt*-MAh and (**b**) the types of FPOCs including 15 phr of graphite

Figure 4 shows the dependence of storage modulus on the angular frequency (ω) for the series of composites prepared with different types of FPOCs. It is seen in these figures that the high and low frequency behavior of composites varied significantly depending on the type of FPOC employed. It is known that the high frequency behavior of polymer composites reflect the rheological behavior of polymer phase and/or polymer-polymer interactions while the low frequency or terminal behavior provides information about filler-polymer or filler-filler interactions in the modulus (G^*, G', G'')-ω curves of polymer composites. Therefore, conclusions about the microstructural features of polymer composites by the rheological measurements such as level of filler dispersion and orientation, A_f, percolation threshold and interfacial issues between polymer chains and filler surface are generally attributed to the low frequency behavior of samples. But, high frequency behavior could be sometimes useful, in particular, to assess the polymer-polymer interactions and processability of samples at high shear rates for the composites which include a secondary polymeric component like compatibilizers, interfacial agents, additives, processing aids etc. In the present study, the rheological behaviors of samples were studied in detail by quantifying the high and low frequency data because the samples contain a relatively high amount of functional copolymers, in terms of polymer blend.

For the sample series of G-x and C2-x given in Fig. 4(a) and (c), respectively, the high frequency modulus of composites (only except of G15) are the same with the G' of COC. This result implies that the rheological behavior of such series of composites was determined by the rheological behavior of COC. This also indicates that the introducing of poly(maleic anhydride-*alt*-1-octadecene) and graphite into the COC phase did not affect the rheological behavior of composites at high frequencies or shear rates. On the other hand, the G' values of the samples series of C1-x, given in Fig. 4(b), increases with the increasing amount of graphite and poly(isobutylene-*alt*-maleic anhydride) at high frequency region. On the other hand, the G' values of the samples series of C1-x, given in Fig. 4(b), increases with the increasing amount of graphite and poly(isobutylene-*alt*-maleic anhydride) at high frequency region. For this series of sample, the composites exhibit higher G' values than the COC in the entire range of frequency employed and the G' value increases with the increasing amount of graphite at a given frequency. Frequency dependence of G' for the sample series of C3-x prepared with the poly(ethylene-*graft*-maleic anhydride) is seen in Fig. 4(d). These samples show different behavior at high and low frequency region depending on the composition. Interestingly, introducing the more poly(ethylene-*graft*-maleic anhydride) into the composition slightly reduced the high frequency modulus of the composite. Furthermore, increasing amount of 2D, layered filler, graphite, cannot compensate this decrease in modulus. This behavior

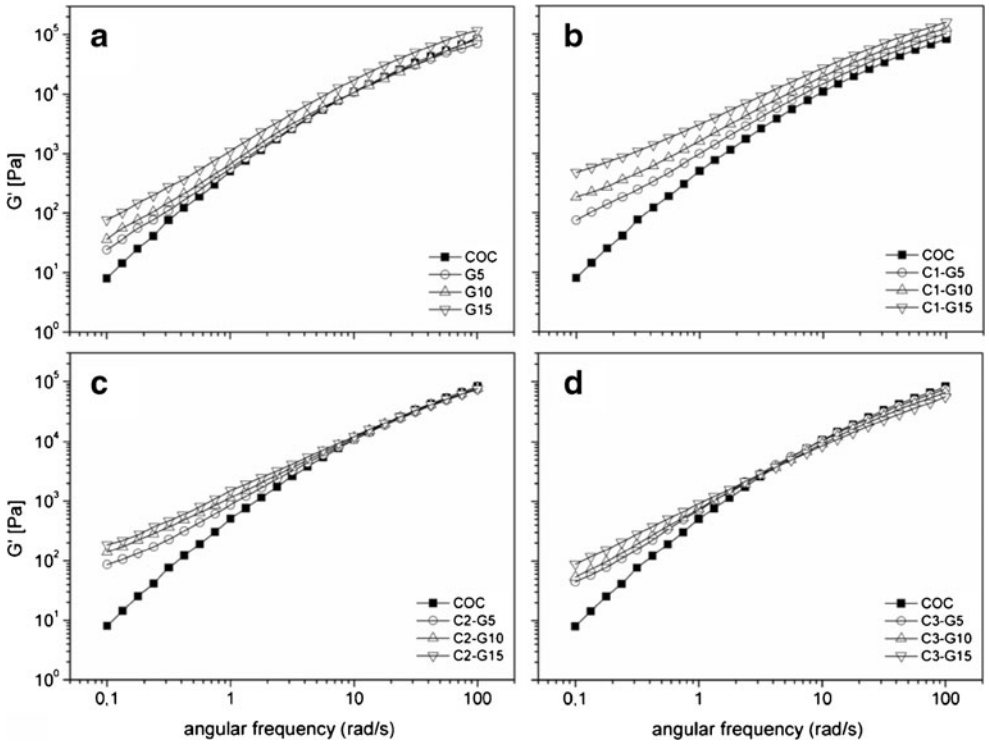

Fig. 4 Storage modulus (G') as a function of angular frequency (ω) for the samples series prepared with (**a**) no FPOCs, (**b**) PiB-*alt*-MAh, (**c**) PMAh-*alt*-1-OD and (**d**) PE-*g*-MAh

could be attributed to the fact that no interaction is present between the COC and poly(ethylene-*graft*-maleic anhydride) and these polymers are partly immiscible.

Figure 5 shows the values of high and low frequency modulus (G'_{100} and $G'_{0.1}$) to compare the effect of copolymer type on the relative change in G′, more precisely. Variation in both G'_{100} and $G'_{0.1}$ contingently exhibit zig-zag plots since the *x*-axes of the curve was constituted by the sample denotations. Peak and pit points of the plots pertain to the samples of C1-x and C3-x, respectively. Values of the G'_{100} and $G'_{0.1}$ increases with the increasing amount of graphite and poly(isobutylene-*alt*-maleic anhydride) whereas the values of G'_{100} slightly decrease with the increasing amount

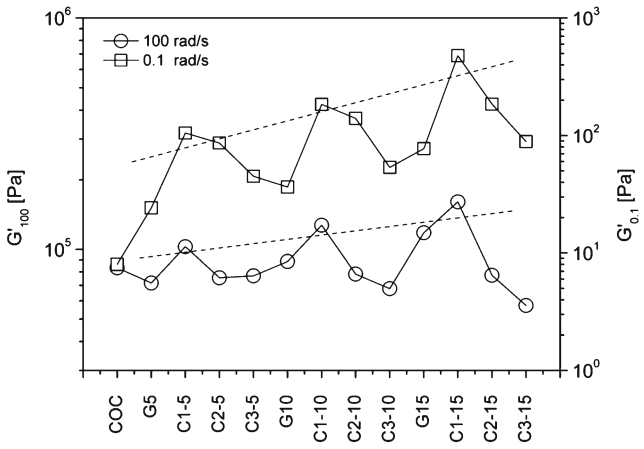

Fig. 5 Values of low and high frequency modulus (G') of samples

of graphite and poly(ethylene-*graft*-maleic anhydride) for the samples series of C3-x.

Another rheological parameter is the low frequency or terminal regime exponent (Γ) for comparing the filler-filler or polymer-filler interactions of various composite systems. This parameter has been frequently used to determine the rheological percolation threshold of the polymer composites depending on the volume fraction of filler [40–42]. Percolation threshold is physically defined as the critical volume fraction of fillers for the formation of a three-dimensional network [43]. Rheological approaches used to determine the percolation threshold are generally based on the contributions of hydrodynamic volume occupied with an individual filler particle or aggregates. But, in this study, we used the parameter, Γ, to compare the effects of type and chemical structure of FPOCs on the interfacial interactions between the graphite and COC. Figure 6 illustrates the experimental values of terminal regime exponent (Γ), determined in the frequency range of 0.1–0.5 rad/s, for the different series of samples. Lower Γ values could be attributed to the higher interfacial interaction between the COC and graphite flakes. Considering the Γ plots of the series of samples given in Fig. 6, it can be concluded that the interfacial interaction between the COC and graphite flakes decreased in the order of C1-x>C2-x>C3-x. This relationship also indicates that the poly(isobutylene-*alt*-maleic anhydride) is the most effective polymeric additive as clearly observed in the SEM analysis of the samples. This analysis also implies that all compositions were below the rheological percolation since the Γ plots showed a single slope for the amount of graphite

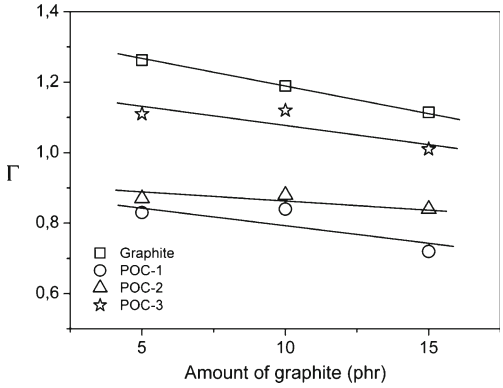

Fig. 6 Dependence of slope of storage modulus (G') curves at low frequency region (Γ) as a function of graphite amount for the sample series

studied. Mirzazadeh et al. reported that PP-*g*-MA yielded higher level of interaction between PP and EG than EPDM-*g*-MA as compatibilizer [44]. But in this study, it was found that the maleic anhydride grafted polyethylene (PE-*g*-MA) did not yield an effective interaction between the COC phase and graphite flakes on the contrary to other polyolefin systems.

DSC curves of the samples are illustrated in Fig. 7. It is seen in the Fig. 7(a) that the glass transition temperature (T_g) of COC was found to be 78.0 °C as declared by the producer. It was found that the T_g values of COC/graphite samples prepared without a compatibilizer slightly increased by introducing of graphite sheets into the composition as given in Fig. 7(a). This is probably due to the restriction effect of graphite sheets on the mobility of COC segments. On the other hand, different relationship was observed in the variation of the values of T_g depending on the sample composition for the series of samples prepared with various types of FPOCs. Figure 7(b), (c) and (d) show the DSC curves of the sample series prepared with the poly(isobutylene-*alt*-maleic anhydride), poly(maleic anhydride-*alt*-1-octadecene) and poly(ethylene-*graft*-maleic anhydride), respectively. In all sample series, the T_g of COC decreased with the increasing amount of filler. But, it can be assumed that this effect was originated from the increasing amount of FPOC into the composition. This influence is more pronounced for the sample series prepared with the PE-*g*-MA. The T_g of the C3-G15 sample was found to be about 6 °C lower than that of COC. In Fig. 7(d), the melting endotherm of PE-*g*-MA are also seen in the temperature range of 90–110 °C.

Dynamic mechanical analysis results, changes in the storage and loss modulus (E', E'') and loss factor (Tanδ=E''/E') of the COC and the sample series of C1-x as a function of temperature are given in Fig. 8(a) and (b), respectively. It is well known that DMA is a widely used and rapid tool for precisely probing relaxation issues in polymers, blends and composites and characterization of their viscoelastic properties in the solid state. The glassy plateau and glass transition region are clearly seen in these curves. It was obtained that the storage modulus (E') of the composites below the glass transition temperature (T_g) increases substantially with the increasing amount of graphite and FPOC due to the stiffening

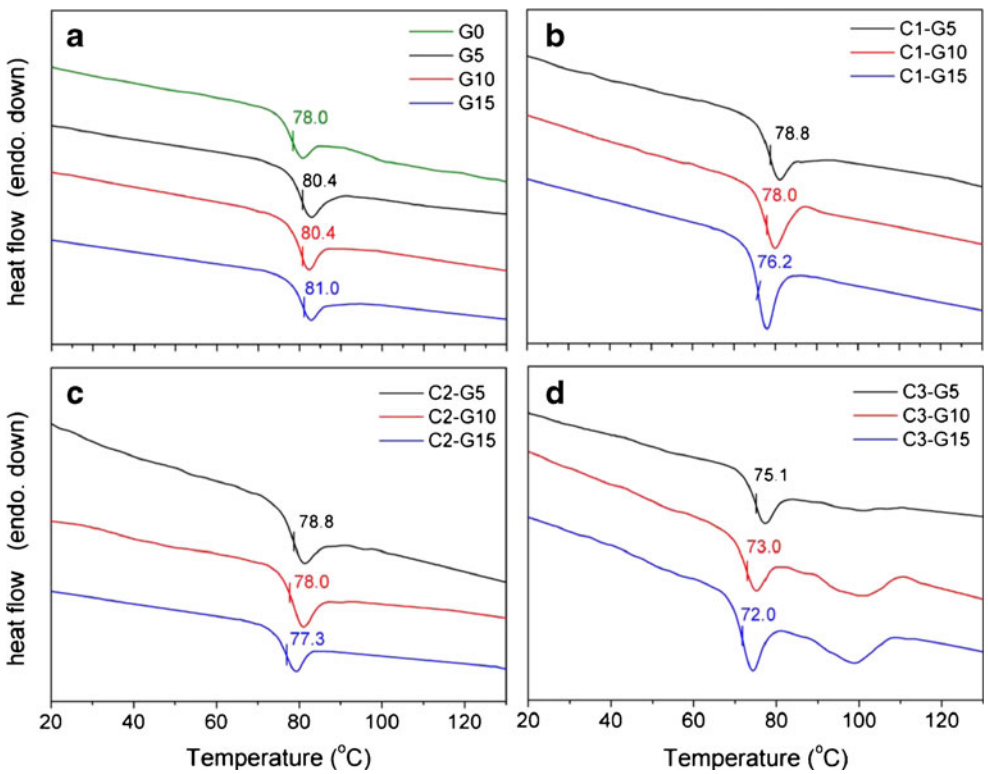

Fig. 7 DSC curves of the series of samples at the glass transition region of COC. Samples prepared with (**a**) no compatibilizer, (**b**) poly(isobutylene-*alt*-maleic anhydride), (**c**) poly(maleic anhydride-*alt*-1-octadecene) and (**d**) poly(ethylene-*graft*-maleic anhydride)

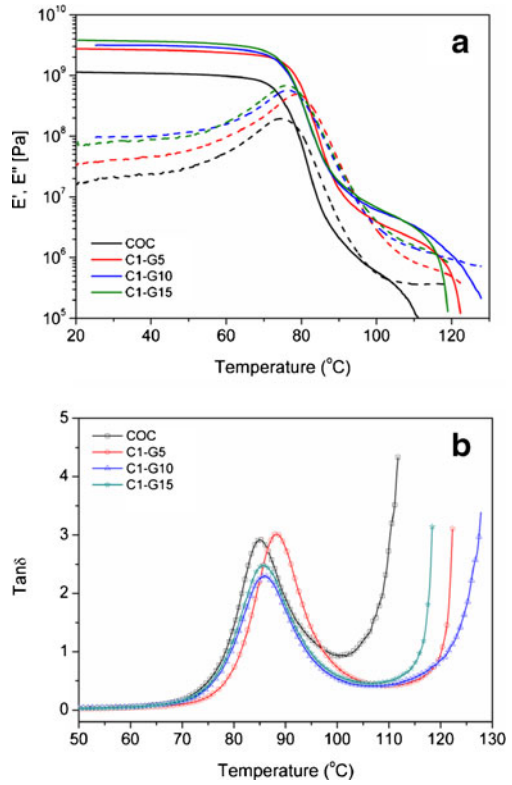

Fig. 8 DMA curves of the sample series prepared with the PiB-*alt*-MAh. (**a**) Dependence of storage (E') and loss modulus (E'') and (**b**) phase angle (Tanδ) on the temperature

effect of layered graphite flakes. Similar trend was obtained for the other series of samples but not given here. Although peak maxima of Tanδ [Fig. 8(b)] can be generally regarded as the glass-transition (T_g) temperature, in the present study transition temperature from the glassy plateau to rubbery region in the E' curve was taken as the T_g because this transition is consistent with the reported value in the data sheet of COC and the measured one with the DSC analysis (78.0 °C). Based on the DMA tests, the T_g values of the G5, C1-5, C2-5 and C3-5 were found to be 81.0, 77.6, 75.6 and 78.0 °C, respectively. It can be generally said that the composite samples prepared without FPOC exhibited higher T_g values than the COC whereas the composites including various types and amounts of FPOCs showed lower T_g values. The DMA analysis implied the same trend with the DSC results for the T_g values of samples depending on the composition. The T_g values of the composites varied in the temperature range of 76–81 °C in the DMA analysis. It was also observed that the T_g values were more influenced by the types and amounts of FPOCs rather than the filler amount as well as mentioned in the part of DSC analysis before.

Improvement in the storage modulus (E') of the samples is given in Fig. 9 depending on the type and amount of FPOC and the amount of graphite. The E' values, compared in this figure,

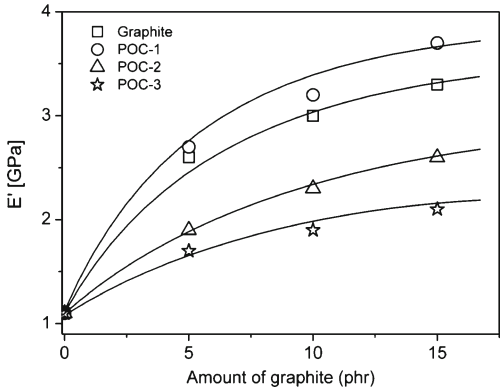

Fig. 9 Improvement in storage modulus (E') values of the samples at 30 °C depending on the amount of graphite and the type of FPOCs

are the modulus values of the samples at the temperature of 30 °C. Storage modulus of polymer matrix, COC, was 1.1 GPa at this temperature. It was found that the poly(isobutylene-*alt*-maleic anhydride) yielded higher E' values than the samples prepared without a copolymer, G-x, at a given graphite amount. On the other hand, the series of samples prepared with the poly(maleic anhydride-*alt*-1-octadecene) and poly(ethylene-*graft*-maleic anhydride) copolymers showed lower E' values than the G-x. Storage modulus values of the series of samples decreased in the order of C1-x>G-x>C2-x>C3-x.

Gas permeability

Nitrogen permeability (P) values of the film samples are listed in Table 3. It is seen that the addition of 5 phr of graphite reduced the P value of COC about 42–48 %. This improvement is almost independent from the type of polyolefin copolymer which indicates that the gas permeability of COC/graphite

Table 3 Gas permeability values of the COC and COC/graphite composite films

Samples	P (cc.100 μ/m^2.day.bar)
G0	134
G5	78
G10	57
G15	54
C1-G5	70
C1-G10	53
C1-G15	51
C2-G5	75
C2-G10	55
C2-G15	52
C3-G5	78
C3-G10	61
C3-G15	57

composite is more related to the dispersion of graphite stacks into the COC phase than the interfacial interactions.

Therefore, it is obviously inferred that the improvement in barrier performance of the COC/graphite films only originated from the amount of filler and level of dispersion and thus the tortuosity approach can be applied to the permeability data.

One of the most widely used approaches for quantitatively predicting the decrease in permeability of a diffusing molecule in a polymer containing impermeable fillers, is the Nielsen model [45]. The Nielsen model assumes that a two dimensional diffusion occurs through a polymer containing infinitely long, rectangular-cross-section plates that were uniformly dispersed in the matrix but were placed normal to the direction of gas transfer path. Because a diffusing gas molecule cannot permeate the graphite platelets, it must go around them thus leading to a tortuous path.

Nielsen model is defined as;

$$\frac{P}{P_0} = \frac{1-\phi}{1+\left(A_f/2\right)\phi}$$

where P is the permeability value of composite, P_0 is the permeability value of polymer, ϕ is the volume fraction of filler and A_f is the aspect ratio of filler. Model parameters are only the amount of filler and degree of dispersion. It can be clearly predicted from the equation that the relative permeability (P/P_0) decreases with the increasing of aspect ratio (level of dispersion or exfoliation) and amount of filler. Relationship between the relative permeability and volume fraction of graphite is given in Fig. 10. By applying the Nielsen model to the experimental nitrogen permeability data, it was found that the A_f values of the graphite flakes reduced with the increasing amount of filler and FPOC for the all sample series. The highest A_f values (approximately 60–80) were obtained with the 5 phr of graphite. Nielsen model suggested the average A_f values in the range of 50–60 and 40–50 for the series of samples including 10 phr and 15 phr of graphite, respectively. For a given amount of graphite, the C1-x samples possesses slightly lower P values than the other series of samples which suggests higher aspect ratio. Estimation of aspect ratio for the graphite flakes is very consistent with those obtained from the direct observation in the sample morphology and SEM images analysis.

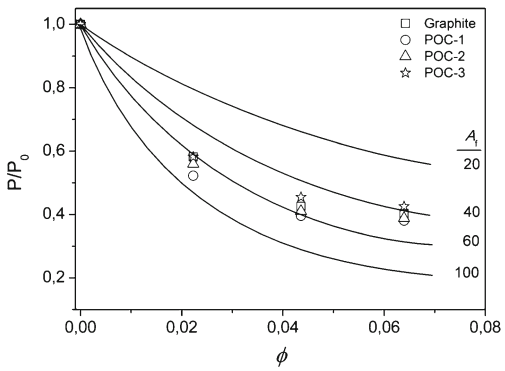

Fig. 10 Nielsen model applied to the gas permeability data of samples for estimating the average aspect ratio of graphite flakes

Conclusions

In this study, it has been shown that the interfacial interaction between a hydrophobic polymer matrix and natural graphite surfaces was quite different from other composite system. The most commonly used compatibilizer, poly(ethylene-*graft*-maleic anhydride), in the polymer blend and composite systems was found to be an inefficient additive for the COC/graphite composites whereas the poly(isobutylene-*alt*-maleic anhydride) yielded a strong interfacial interaction and adhesion between the graphite flakes and COC phase. This can be attributed to the differences in molecular structure of copolymers. Functionality of a POC mainly depends on the content or the graft ratio (w/w%) of *co*-monomer. The poly(isobutylene-*alt*-maleic anhydride) and poly(maleic anhydride-*alt*-1-octadecene) are alternating copolymers while the poly(ethylene-*graft*-maleic anhydride) is graft copolymer. It is well known that the maleic anhydride groups are generally grafted on chain ends of polyethylene. Considering the acid number values given in Table 1, one can normally expect that an alternating copolymer includes more maleic anhydride groups than a graft copolymer. On the other hand, poly(isobutylene-*alt*-maleic anhydride) yielded a strong interfacial interaction and adhesion between the graphite flakes and COC phase. But, the poly(maleic anhydride-*alt*-1-octadecene) also yielded poor interfacial adhesion and immiscible structure with the COC which could be originated from relatively long chain branching of octadecene groups. On the other hand, it was found that the poly(isobutylene-*alt*-maleic anhydride) copolymer yielded a significant interfacial adhesion in the COC-graphite interface and showed no clear immiscibility. These could be attributed to the relatively low molecular weight and high glass transition temperature of this copolymer. Consequently, the poly(isobutylene-*alt*-maleic anhydride) copolymer can be used to prepare high performance COC/natural graphite composites with improved mechanical properties.

Acknowledgments This study was supported by TÜBİTAK, The Scientific and Technological Research Council of Turkey, with the grant number of 110 M671 and The Turkish Ministry of Development (formerly DPT) with the grant number of 2008 K121000. Authors also acknowledged to Dr. Raffaele Gilardi from the TIMCAL Graphite & Carbon Company (Switzerland) for kindly supplying the graphite used in this work and Mr. Vedat Sariboga and Mr. Hasan Özdemir from the Department of Chemical Engineering at Istanbul University (Turkey), for their efforts and helps in the SEM study.

References

1. Stankovich S, Dikin DA, Dommett GHB, Kohlhaas KM, Zimney EJ, Stach EA, Piner RD, Nguyen SBT, Ruoff RS (2006) Nature 442:282–286
2. Sengupta R, Bhattacharya M, Bandyopadhyay S, Bhowmick AK (2011) Prog Polym Sci 36:638–670
3. Kuilla T, Bhadra S, Yaho D, Kim NH, Bose S, Lee JH (2010) Prog Polym Sci 35:1350–1375
4. Kim H, Abdala AA, Macosko CW (2010) Macromol 43:6515–6530
5. Chiang C-L, Hsu S-W (2010) J Polym Res 17:315–323
6. Martin-Gallego M, Verdejo R, Lopez-Manchado MA, Sangermano M (2011) Polymer 52:4664–4669
7. Zaman I, Phan TT, Kuan H-C, Meng Q, La LTB, Luong L, Youssf O, Ma J (2011) Polymer 52:603–1611
8. Tsai K-C, Kuan H-C, Chou H-W, Kuan C-F, Chen C-H, Chiang C-L (2011) J Polym Res 18:483–488
9. Mahmoud A-G, Pötschke P, Zhou D, Mark JE, Heinrich G (2007) J Macromol Sci Part A Pure and Appl Chem 44:591–598
10. Hu Z, Liu C (2013) J Polym Res 20:39–46
11. Al-Hartomy OA, Al-Salamy F, Al-Ghamdi AA, Fatah MA, Dishovsky N, El-Tantawy F (2011) J Appl Polym Sci 120:3628–3634
12. Hubert PJ, Kathiresan K, Wakabayashi K (2011) Polym Eng Sci 51:2273–2281
13. Wang L, Hong J, Chen G (2010) Polym Eng Sci 50:2176–2181
14. Kim H, Kobayashi S, AbdurRahim MA, Zhang MJ, Khusainova A, Hillmyer MA, Abdala AA, Macosko CW (2011) Polymer 52:1837–1846
15. Lian H, Li S, Liu K, Xu L, Wang K, Guo W (2011) Polym Eng Sci 51:2254–2260
16. Yoonessi M, Gaier JR (2010) ACS Nano 4:7211–7220
17. Kim H, Macosko CW (2009) Polymer 50:3797–3809
18. Rusu G, Rusu E (2007) J Optoelectro Advan Mater 9:2102–2109
19. Liu Y, Chen Z, Yang G (2011) J Mater Sci 46:882–888
20. Du N, Zhao C-Y, Chen Q, Wu G, Lu R (2010) Mater Chem Phys 120:167–171
21. Xia L-H, Li A-J, Wang W-G, Yin Q, Lin H, Zhao Y-B (2008) J Power Source 178:363–367
22. Zhang M, Li D-J, Wu D-F, Yan C-H, Lu P, Qiu G-M (2008) J Appl Polym Sci 108:1482–1489
23. Li ML, Jeong YG (2011) Compos Part A Appl Sci and Manufac 42:560–566
24. Zhang H-B, Zheng W-G, Yan Q, Yang Y, Wang J-W, Lu Z-H, Ji G-Y, Yu Z-Z (2010) Polymer 51:1191–1196
25. Kim H, Macosko CW (2008) Macromol 41:3317–3327
26. Bian J, Wei XW, Lin HL, Wang L, Guan ZP (2012) J Appl Polym Sci 124:3547–3557
27. Zhang H-B, Zheng W-G, Yan Q, Jiang Z-G, Yu Z-Z (2012) Carbon 50:5117–5125
28. Wu T-C, Tsai K-C, Lu M-C, Kuan H-C, Chen C-H, Kuan C-F, Chiu S-L, Hsu S-W, Chiang C-L (2012) J Compos Mater 46:1483–1496
29. Kim K-S, Park S-J (2011) Bull Korean Chem Soc 32:196–200
30. Cai D, Song M (2009) Nanotechnology 20:315708
31. Cerezo FT, Preston CML, Shanks RA (2007) Macromol Mater Eng 292:155–168
32. Mirzazadeh H, Katbab AA, Hrymak AA (2011) Polym Adv Technol 22:863–869
33. Fink JK (2010) Handbook of engineering and speciality thermoplastics. Scrivener Publish, Massachusetts
34. Qu CF, Hsu MC (2007) J Appl Polym Sci 104:2542–2548
35. Dorigato A, Pegoretti A, Fambri L, Slouf M, Kolarik J (2011) J Appl Polym Sci 119:3393–3402
36. Qu CF, Hsu MC (2008) J Appl Polym Sci 110:732–737
37. Dorigato A, Pegoretti A, Migliaresi C (2009) J Appl Polym Sci 114:2270–2279
38. Motlagh GH, Hyrmak AN, Thompson MR (2007) J Polym Sci, Part B: Polym Phys 45:1808–1820
39. Kasgoz A, Akın D, Durmus A (2012) Polym Eng Sci 52:2645–2653
40. Jeon HS, Rameshwaram JK, Kim G, Weinkauf DH (2003) Polymer 44:5749–5758
41. Zhao J, Morgan AB, Harris JD (2005) Polymer 46:8641–8660
42. Shen L, Lin Y, Du Q, Zhong W, Yang Y (2005) Polymer 46:5758–5766
43. Kirkpatrick S (1973) Rev Modern Phys 45:574–588
44. Mirzazadeh H, Katbab AA, Hrymak AN (2011) Polym Adv Technol 22:863–869
45. Nielsen LE (1967) J Macromol Sci Part A Chem 1:929–942